5-2024

A parametric study on the energy dissipation capability of frictional mechanical metamaterials engineered for vibration isolation

Shayan Khosravi
The University of Texas Rio Grande Valley

Mohsen Amjadian
The University of Texas Rio Grande Valley, mohsen.amjadian@utrgv.edu

Recommended Citation

Khosravi, S., and M. Amjadian. "A parametric study on the energy dissipation capability of frictional mechanical metamaterials engineered for vibration isolation." In Active and Passive Smart Structures and Integrated Systems XVIII, vol. 12946, pp. 229-239. SPIE, 2024. https://doi.org/10.1117/12.3010913

A Parametric Study on the Energy Dissipation Capability of Frictional Mechanical Metamaterials Engineered for Vibration Isolation

S. Khosravi[a] and M. Amjadian[1a]
[a] Department of Civil Engineering, The University of Texas Rio Grande Valley, 1201 W University Dr, Edinburg, TX, USA 78539.

ABSTRACT

Mechanical metamaterials are engineered structures with complex geometric arrangements that display unconventional mechanical properties which are uncommon in traditional materials. They possess the ability to manipulate and control mechanical wave propagation across specific frequency ranges known as frequency bandgaps. This feature makes them extremely useful for a variety of applications in structural control including passive vibration isolation. These materials can be engineered to selectively block or redirect the input motion at their dominant frequency while allowing the transmission of motion at other frequencies. This paper aims to study the dynamic performance of an innovative mechanical metamaterial designed for seismic isolation in multi-story buildings. This seismic isolator, which is termed the meta-isolator (MI), utilizes solid friction to enhance energy dissipation in addition to its natural viscous damping. The proposed MI comprises multiple interconnected cells linked in series via a network of springs and dampers, where each cell includes a lumped mass, spring, damper, and sliding surface, providing both vibration isolation and energy dissipation functionalities. A dynamic model is developed to characterize the nonlinear hysteresis behavior of the proposed MI. This model is implemented on a one-story building model to assess its seismic performance under specific ground motion. A parametric analysis is conducted to optimize the key parameters of both the MI and the building model aiming to reduce drift and absolute acceleration responses. These parameters include mass and frequency ratios, the magnitude of normal force acting on the sliding surface within each cell, and the number of cells. Finally, the optimized dynamic model of the MI is utilized to evaluate its efficacy in seismic isolation of a finite element (FE) model of a one-story 2D frame building subjected to the same ground motion. The FE model is developed using the OpenSEESPy package which is a Python 3 interpreter for OpenSEES. Insights from this study indicate significant promise for the performance of the proposed MI offering hope for its use as a potent passive control system for seismic isolation. In particular, we have shown that lightweight MIs with low frequency ratios (less than 0.5) can outperform the conventional seismic isolators.

Keywords: Mechanical Metamaterials, Frequency Band Gap, Vibration Isolation, Energy Dissipation, Friction.

1. INTRODUCTION

Over the last decade, mechanical metamaterials and their unique structural properties have been the subject of extensive research for various applications, particularly for vibration control of dynamic systems in structural and mechanical engineering. This is due to the unconventional features that these materials exhibit for the propagation of solid waves, making them ideal for a wide range of applications in vibration control, including vibration isolation [1]. These unique features result from their mechanical parameters and periodic geometrical configurations, which play a key role in improving their dynamic characteristics, such as natural damping and frequency [2].

The concept of seismic isolation is well-established in structural engineering [3]. It has been utilized to mitigate seismic lateral loads in multi-story buildings and highway bridges through the implementation of various types of seismic isolators, such as Elastomeric Rubber Bearings (ERBs), Lead-Rubber Bearings (LRBs), and Friction Pendulum Systems (FPSs) [3]. The fundamental idea behind seismic isolation is to reduce the input seismic energy by

[1]mohsen.amjadian@utrgv.edu; phone (956)665-5880; https://www.insdslab.com/.

Active and Passive Smart Structures and Integrated Systems XVIII, edited by Serife Tol, Guoliang Huang, Xiaopeng Li, Mostafa A. Nouh, Shima Shahab, Jinkyu Yang, Proc. of SPIE Vol. 12946, 1294615 · © 2024 SPIE · 0277-786X · doi: 10.1117/12.3010913

shifting the fundamental frequency of the primary structure away from the predominant frequency of the ground motion while simultaneously enhancing the primary structure's damping capacity.

The recent advancements in manufacturing of mechanical metamaterials along with the fact that they are very flexible to design, have opened up a new frontier for the design of seismic isolation in civil structures (see Figure 1). The basic concept behind the design of these materials for seismic isolation is based on creating a frequency bandgap to filter out the predominant frequency of ground motion while simultaneously absorbing the seismic energy input [4]. For this reason, significant efforts have been dedicated to designing new types of mechanical metamaterials for vibration isolation.

Figure 1. Schematic view of a type of mechanical metamaterial used for seismic isolation of a short-story building.

Reynolds and Daley (2014) developed a new type of vibration isolator based on elastodynamic metamaterial which exhibited a double negative behavior for mass and stiffness in a passive manner. Then they incorporated active control to design an active vibration isolator with enhanced frequency bandgap effects [5]. Wang et al. (2019) proposed a local resonant rod with high-static-low-dynamic-stiffness (HSLDS) resonators to develop a low-frequency band gap to filter longitudinal wave propagated along the length of the rod. They studied the effects of damping and nonlinearity of the HSLDS resonator on the dispersion capability of the proposed local resonant rod. They showed that the proposed isolation technique can be considered as a potential solution for manipulation and filtering out of low frequency wave in elastic rods [6]. Gao et al. (2019) investigated band-gap properties of non-uniform infinite periodic beams using numerical and experimental methods. They studied the band-gap properties of such beams based on the Euler–Bernoulli and the Timoshenko theories for elastic beams. They found out that the band-gap boundaries calculated by the Timoshenko beam theory are smaller than those obtained using the Euler–Bernoulli beam theory [7]. Masoom et al. (2023) proposed a two-dimensional periodic foundation system with steel-silicone embedded assemblies to serve as local resonators. The proposed foundation can cover a wide and ultra-low frequency region in its band gap, enveloping the principal frequencies of seismic waves (i.e., 0.2 Hz to 10 Hz). Results of attenuation in the bandgap have been obtained theoretically and experimentally [8]. Chondrogiannis et al. (2020) investigate finite lattice configurations, which consist of impact damper unit cells. They conducted a parametric study on a one-dimensional lattice comprising a finite number of unit cells. The study considered variable parameters, such as the number of unit cells, stiffness, and mass ratio. Their findings demonstrated that the proposed method significantly impacts the base meta structure, leading to effective vibration mitigation [9]. Lv et al. (2024) proposed a metamaterial based on Coulomb friction is self-recoverable and reusable. They provided an analytical formula for the structure's energy consumption. The metamaterial structure consists of an external I-shaped structure and a buckle-like structure composed of a plug and cantilever beams inside. This kind of metamaterial has the potential to be used in the production of multi-functional metamaterial structures such as reusable bumpers [10]. In a recent research, Banerjee et al. (2022) studied vibration transmission through the frictional mass-in-mass metamaterial using an analytical approach. They employed a linear complementary-based Euler discretization algorithm to simulate the dynamics of the system in the presence of friction. The authors observed that a wide low-frequency bandgap can be obtained in the proposed frictional metamaterial for a medium range of frictional force [11].

The objective of this paper is to investigate the dynamic behavior of a novel mechanical metamaterial designed for seismic isolation in multi-story buildings. This seismic isolator, termed as meta-isolator (MI), leverages solid friction to enhance its energy dissipation capacity. It comprises several interconnected cells which are connected in series through a network of springs and dampers. Each cell consists of a lumped mass, spring, damper, and a sliding surface, engineered to provide both vibration isolation and energy dissipation. The dynamic behavior of the system is characterized by developing the equation of motion of the system in terms of the key parameters of a unit cell. These parameters are optimized through a parametric study to tune the system's resonance frequency while concurrently optimizing the friction and normal force to enhance energy dissipation. The optimized MI will then be used to evaluate its effectiveness in seismic base isolation of a one-story 2D frame building subjected to a given earthquake excitation using the OpenSEESPy package in Python.

2. DYNAMIC MODEL

2.1. Configuration of the Proposed Meta-Isolator

Figures 2(a) and 2(b) show the implementation of proposed MI on a one-story building described by a SDOF system with the mass, damping, and stiffness coefficients: M_s, C_s, and K_s, respectively. This dynamic system is subjected to an earthquake along the u-axis with the horizontal ground acceleration $\ddot{u}_g$.

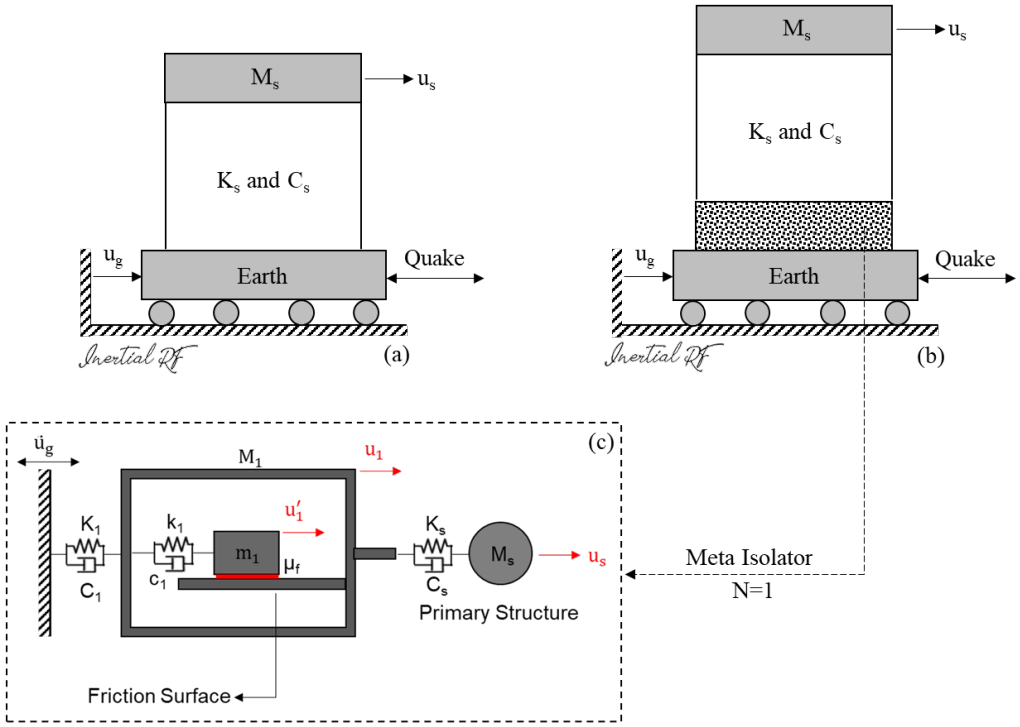

Figure 2. Proposed MI used for seismic isolation of a SDOF system: (a) no isolation, (b) with isolation, and (c) MI with a single cell (N=1).

Figure 2(c) shows the key components of MI with a single cell (N=1). The dynamic system of cell is represented by a 2-DOF model consisting of a rigid container (cell) with the mass M_1 whose left end is attached to the ground through a viscoelastic connection with the stiffness and damping coefficients K_1 and C_1, respectively. The other end of the cell is connected to the primary mass. The cell contains an intercellular oscillator (resonator) with the mass m_1 which is connected to cell through a viscoelastic connection with the stiffness and damping coefficients k_1 and c_1, respectively, and a friction surface with the sliding friction coefficient μ_f. The displacements of the primary mass, the cell, and the resonator are denoted by u_s, u_1, and u'_1 as shown in Figure 2(c). The dynamic system, including the primary mass and the single-cell MI (N=1), overall has 3 DOFs. The effectiveness of the proposed MI in reducing vibrations in the primary structure can be enhanced by increasing the number of cells ($N \geq 1$) and adding additional degrees of freedom (DOFs).

2.2. Equation of Motion

The governing equation describing the motion of the primary mass and the nonlinear vibration of the MI with a single cell (N=1) when subjected to an earthquake along the u-axis with the horizontal ground acceleration $\ddot{u}_g$ can be written into the following matrix form,

$$\mathbf{M}\ddot{\mathbf{U}} + \mathbf{C}\dot{\mathbf{U}} + \mathbf{K}\mathbf{U} + \mathbf{\Lambda_f} F_f = -\mathbf{M}\boldsymbol{\iota_g}\ddot{\mathbf{u}}_\mathbf{g} \tag{1}$$

where $\mathbf{U} = \{u_s, u_1, u_1'\}^T$ is the displacement vector; $\boldsymbol{\iota}_g = \{1,1,1\}^T$ is the ground acceleration influence vector; $\mathbf{\Lambda}_f = \{0,-1,1\}^T$ is the friction force influence vector; $\mathbf{F}_f$ is the friction force vector; and **M**, **C**, and **K** are the mass, damping, and stiffness matrixes which are defined as,

$$\mathbf{M} = \begin{bmatrix} M_s & 0 & 0 \\ 0 & M & 0 \\ 0 & 0 & m \end{bmatrix}, \mathbf{C} = \begin{bmatrix} C_s & -C_s & 0 \\ -C_s & C_s + C + c & -c \\ 0 & -c & c \end{bmatrix}, \text{and } \mathbf{K} = \begin{bmatrix} K_s & -K_s & 0 \\ -K_s & K_s + K + k & -k \\ 0 & -k & k \end{bmatrix} \tag{2}$$

The damping and stiffness coefficients of the cell, resonator, and the primary structure can be written as,

$$\begin{gathered} C = 2\xi(M+m)\omega, K = (M+m)\omega^2, \\ c = 2\xi' m\omega', k = m\omega'^2, \\ C_s = 2\xi_s m_s \omega_s \; K_s = m_s \omega_s^2 \end{gathered} \tag{3}$$

where ξ and ω are the critical damping ratio and the natural frequency of the cell, respectively, ξ' and ω' are the critical damping ratio and the natural frequency of the resonator, and ξ_s and ω_s are the critical damping ratio and natural frequency of the primary structure. The Coulomb friction model is selected to describe the friction force F_f acting on the resonator [12]:

$$F_f = +\mu_f N_f \times \mathrm{sgn}(\dot{u}_f) \tag{4}$$

where $N_f = m_1 g$ is the normal force acting on sliding surface, and $\dot{u}_f$ is the sliding velocity defined as $\dot{u}_f = \dot{u}_1' - \dot{u}_1$. The friction model described by Equation (4) does not take the stick-slip motion into account[13]. For the cases when $N \geq 1$ we need to update the mass, damping, and stiffness matrices and the friction force vector which for the sake of brevity are not mentioned here, but these cases will be studied in Sections 3-5. In this study, we adopt the assumption that $\mu_f = 0.1$, signifying the utilization of a single material type for the friction surface. However, the friction force can be manipulated by adjusting the mass of the resonator as $N_f = m_1 g$.

Table 1. Dynamic parameters of the one-story building without isolator.

Parameter	Value	Unit
M_s	29485	kg
ω_s	20.944	rad/s
ξ_s	2	%

3. NUMERICAL STUDY

3.1. Numerical Model

The governing equation described by Equation (1) is solved by using MATLAB (Simulink)[14]. In order to characterize the dynamic behavior of the proposed MI and optimize the displacement and acceleration responses of the primary mass the following parameters are defined:

$$f_c = \frac{\omega}{\omega_s}, f_1 = \frac{\omega'}{\omega}, \mu_c = \frac{N(m+M)}{M_s}, \mu_1 = \frac{m}{M} \tag{5}$$

Table 1 lists the corresponding parameters of a one-story building used by Ramallo et al. (2002) in their study on smart base isolation systems [15,16].

3.2. Ground Motion Record

In this study, a far-field ground motion acceleration record is selected from the Pacific Earthquake Engineering Research Center (PEER) database [17]. The key properties of this record are listed in Table 2. For the time-history analysis and parametric study, this record is scaled using the scaling method developed by Hancock et al. (2006) [18]. This adjustment matches the record with the Maximum Considered Earthquake (MCE) design spectrum as defined in the ASCE 7-10 standard [19]. This design spectrum is defined based on a seismic event with a return period of 2475 years, which is specific to a Class B site in California. As can be seen from Figure 3, the scaling process has been carried out for a range of periods from T_n=0.5 s to T_n=5.0 s seconds, ensuring that the modified seismic data accurately reflects the desired seismic performance spectrum for the building [16].

Table 2. Ground motion acceleration record used for the response history analysis [16].

Name	Year	Magnitude (M)	Station	Component	PGA (g)	PGA (g)
Imperial Valley	1979	6.5	Delta	DLT352	0.350	0.384

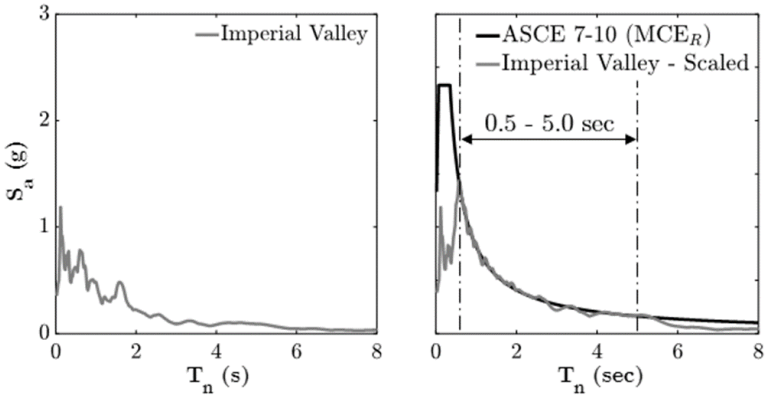

Figure 3. Acceleration response spectra (5% damping) of the ground motion record: (a) un-scaled spectrum (b) scaled spectrum corresponding to the ASCE 7-10 MCE design response spectrum [16].

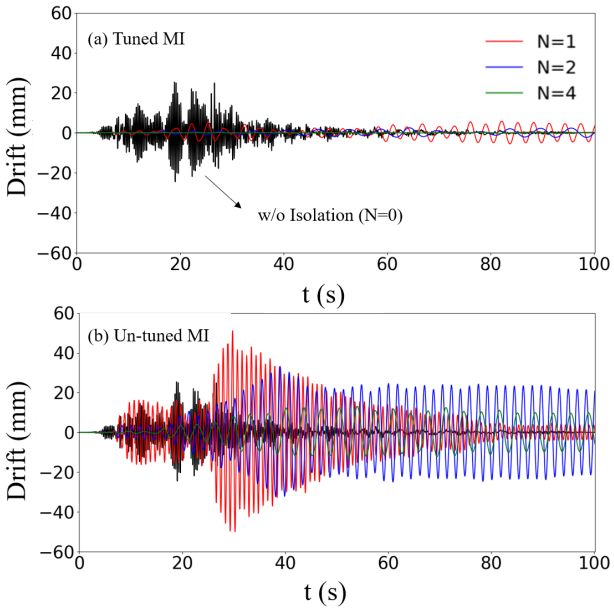

Figure 4. Drift of the primary mass with the proposed MI for N=1, 2, and 4 compared to without isolation case (N=0): (a) tuned MI and (b) untuned MI.

3.3. Preliminary Time-History Analysis

To gain initial insights into the seismic performance of the proposed MI in reducing absolute acceleration and relative displacement of the primary mass of SDOF system as depicted in Figure 2, a preliminary time-history analysis is conducted. The performance of the proposed MI is compared in two cases: (1) Tuned MI: with parameters set as f_c=1, f_l=1, μ_c=0.01, and μ_l=1, and (2) Untuned MI: with parameters set as f_c=3.5, f_l=1, μ_c=0.01, and μ_l=1. In the first case, the MI is tuned to minimize the displacement of the primary mass relative to cell 1 (drift) attached to it. However, in the second case, the MI is not optimally tuned.

Figure 4(a) illustrates the drift of the primary mass for Case 1, demonstrating three distinct cell arrangements with N=1, 2, and 3, respectively, in comparison to the case without isolation. It is evident how the performance of the MI can be enhanced through tuning its parameters properly. The most optimized case is achieved with a higher number of cells. For example, with N=4, a reduction of approximately 90 percent in the maximum drift is achieved, decreasing from 2.75 mm to approximately 0.25 mm. However, for N=1, this reduction is approximately 80 percent. In Figure 4(b), the drift of the primary mass for Case 2 with N=1, 2, and 3 is compared to the case without isolation. The amplification in the response of the primary structure due to mistuning the MI with N=1, 2, and 4 is evident from this figure.

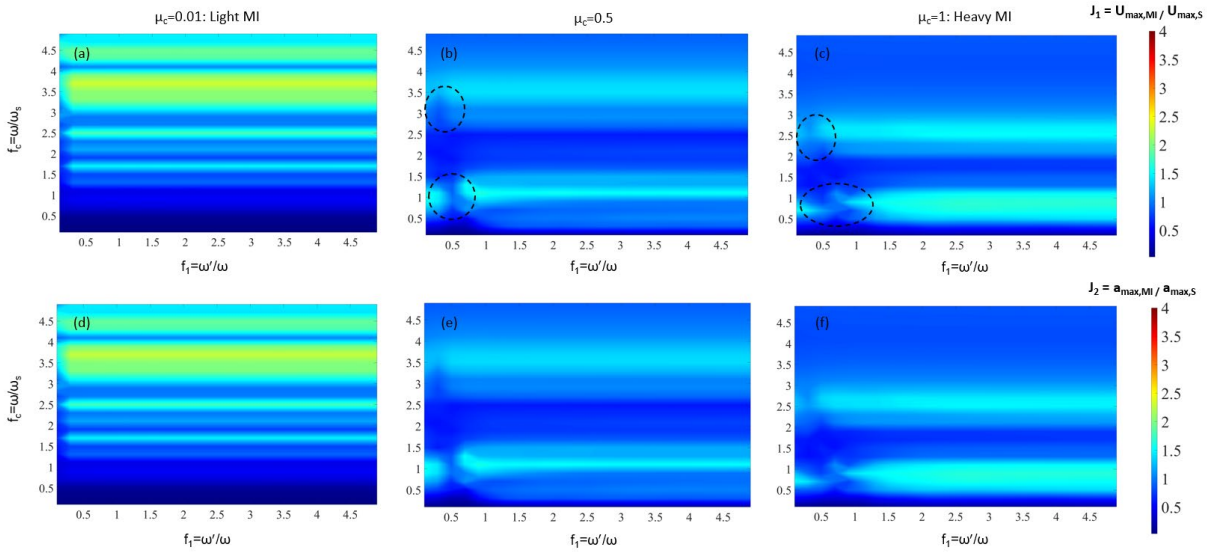

Figure 5. Dynamic response to the proposed MI system under variable mass and frequency ratios for N=1: (a-c) displacement performance index (J_1) for μ_c=0.01, 0.5, 1, and (d-f) acceleration performance index (J_2) for μ_c=0.01, 0.5, 1.

3.4. Parametric Study

In this section, a parametric study is carried out on the key parameters of the proposed MI in order to optimize the seismic performance of the SDOF system. The following two performance indices are defined in order to assess the seismic performance of the MI,

$$J_1 = \frac{\max(|u_s(t) - u_1(t)|)_{N\geq 1}}{\max(|u_s(t)|)_{N=0}} \text{ and } J_2 = \frac{\max(|\ddot{u}_s(t) + \ddot{u}_g(t)|)_{N\geq 1}}{\max(|\ddot{u}_s(t) + \ddot{u}_g(t)|)_{N=0}} \quad (6)$$

where J_1 is the ratio of peak relative displacement of the primary mass with the respect to the MI (N≥1) to the peak displacement of the primary mass without isolation (N=0), J_2 is the ratio of peak absolute acceleration of the primary mass with MI to the corresponding response without isolation.

The key parameters considered in this parametric study are f_c, f_l, μ_c, μ_l, and N. To examine how these variables influence the effectiveness of the proposed MI, we compute the performance indices J_1 and J_2 across a range of f_c and f_l values, changing from 0.1 to 5 with an incremental step of 0.1. In this study, we assess three different values

of μ_c including: 0.01 (representing a light MI), 0.5, and 1.0 (representing a heavy MI). It is also assumed that μ_1=1 indicates that the resonator's mass is set to be equal to the cell's mass.

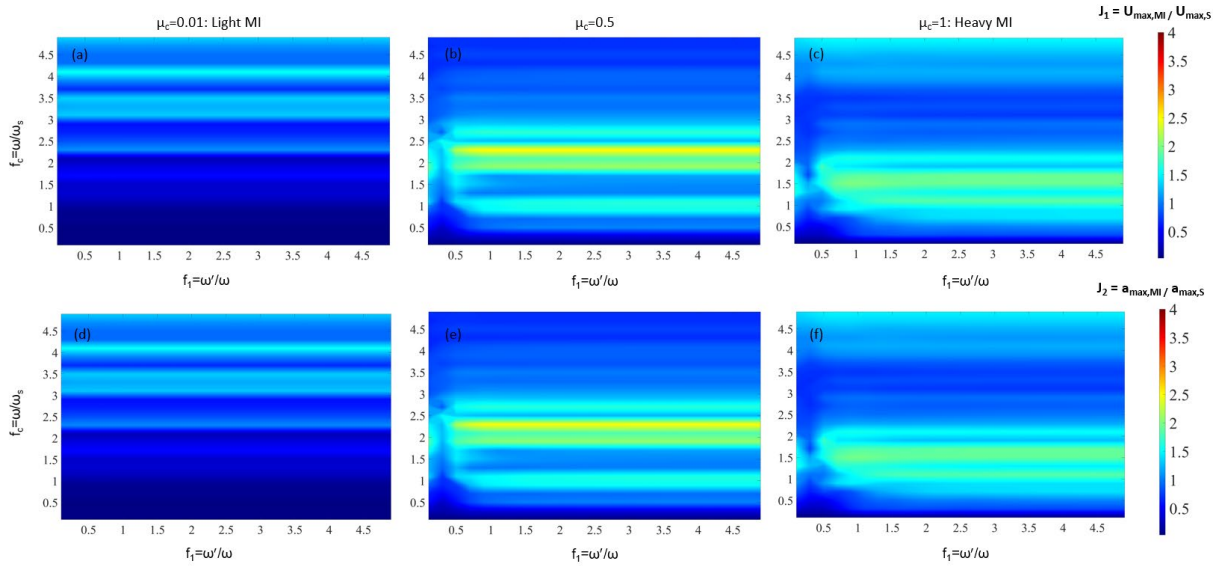

Figure 6. Dynamic response to the proposed MI system under variable mass and frequency ratios for N=2: (a-c) displacement performance index (J_1) for μ_c=0.01, 0.5, 1, and (d-f) acceleration performance index (J_2) for μ_c=0.01, 0.5, 1.

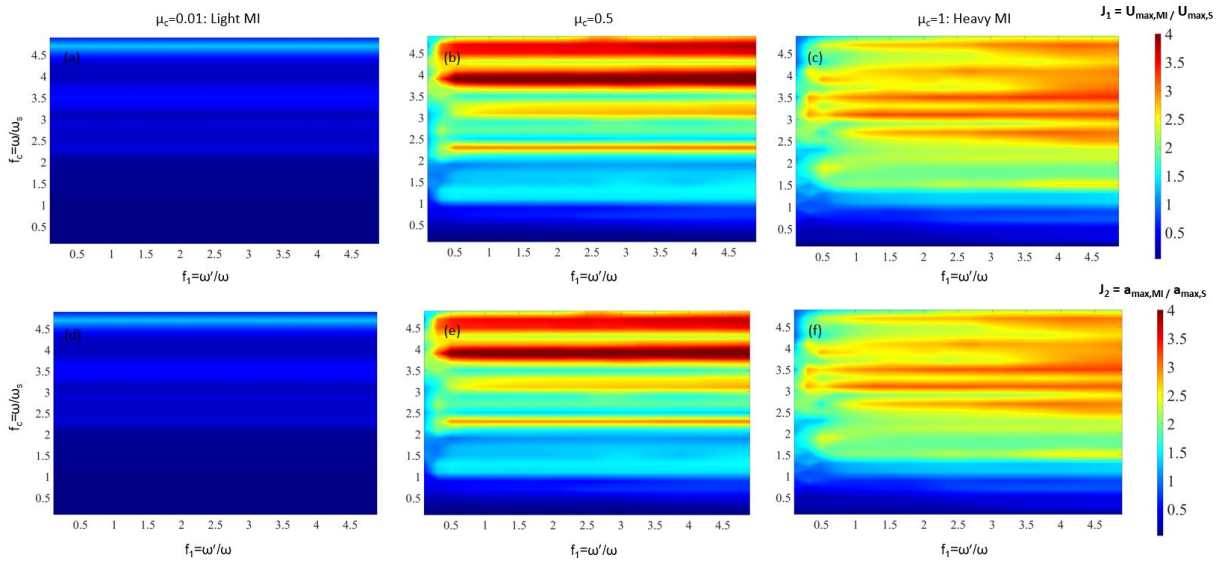

Figure 7. Dynamic response to the proposed MI system under variable mass and frequency ratios for N=4: (a-c) displacement performance index (J_1) for μ_c=0.01, 0.5, 1, and (d-f) acceleration performance index (J_2) for μ_c=0.01, 0.5, 1.

The findings are shown in Figures 5, 6, and 7, corresponding to N=1, 2, and 4, respectively. Figure 5 illustrates that the variations of J_1 and J_2 with respect to f_c and f_1 are similar, as anticipated for seismic isolators, given their comparable efficacy in reducing the absolute acceleration and drift of the superstructure. This observation is also noticeable in Figures 7 and 8 for N=2, and 4, respectively. Furthermore, Figure 5 reveals that the performance of MI is largely unaffected by changes in f_1, but it is notably influenced by f_c and μ_c. It becomes apparent that for a lightweight MI (μ_c=0.01), optimal performance is achieved when f_c approaches a very small value, particularly for f_c<0.5. However, by comparing Figure 5 (N=1) with Figures 6 (N=2) and 7 (N=4), it becomes evident that the performance of lightweight MIs improves with an increase in the number of cells, while for heavier MIs, the performance is notably reduced.

4. FINITE ELEMENT SIMULATION

In this section, we introduce a simple finite element (FE) modeling approach to demonstrate the modeling procedure for the proposed MI using OpenSEESPy [20]. This approach employs a combination of springs and dampers, elements that are widely available in numerous FE software packages.

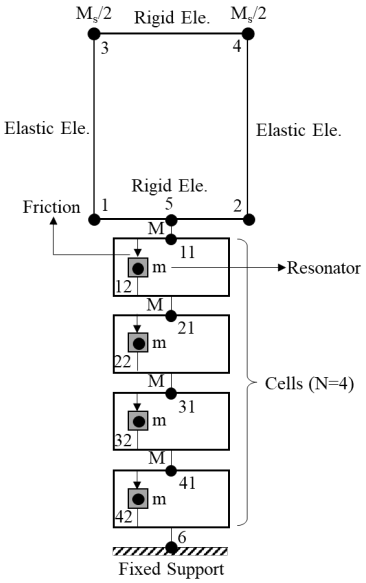

Figure 8. FE model of a one-story 2D frame with the MI (N=4) developed in OpenSEESPy.

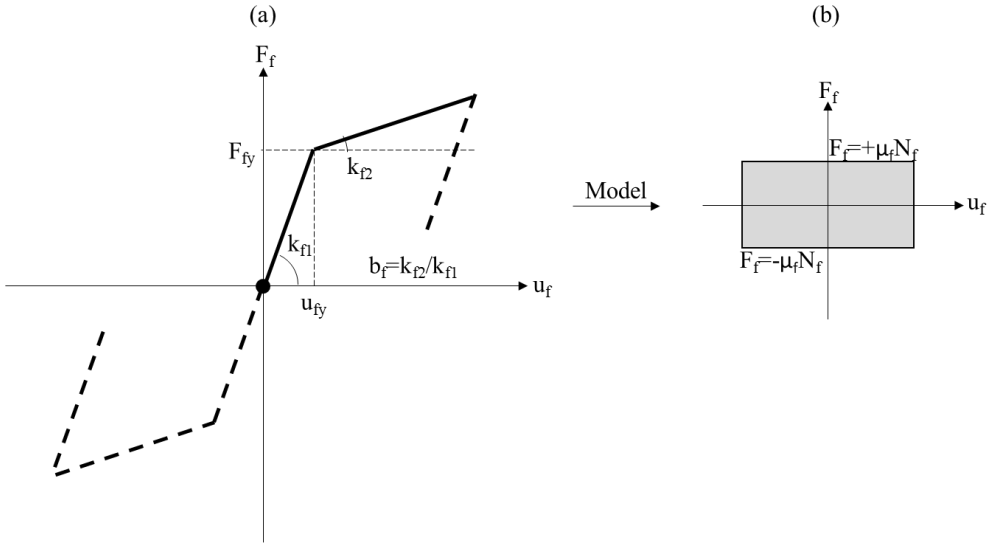

Figure 9. Modeling of force-displacement behavior of friction developed at each cell in OpenSEESPy: (a) Steel-02 material (b) Coulomb friction model[16].

Figure 8 displays the FE model of a one-story 2D frame building equipped with a MI comprising four cells (N=4) in OpenSEESPy. This model represents the SDOF system discussed in Section 3 whose parameters are listed in Table 1. The FE model contains 14 nodes, with nodes 1 to 5 used to model the frame, and the remaining nodes, i.e. nodes {11,12}, {21,22}, {31,32}, and {41,42}, are utilized for modeling cells 1, 2, 3, and 4, respectively. The first cell of the MI is connected to the frame at top and the ground at the bottom through two zero-length elements connecting node 11 to 5 and node 21 to 5, respectively, as shown in Figure 9. The internal nodes (i.e., nodes 12, 22, 32, 42), representing the resonators, are connected to the main nodes of their corresponding cells (i.e., nodes 11, 21, 31, 41)

through two parallel zero-length elements: one exhibiting viscoelastic behavior and the other displaying frictional behavior.

The force-displacement hysteresis behavior of the friction developed at each cell ideally forms a rectangular shape, as depicted in Figure 9(b). To simulate this behavior, the Steel-02 material model in OpenSEESPy, featuring isotropic strain hardening, is utilized. Figure 9(a) illustrates the typical force-displacement hysteresis curve of this material which can be characterized by three parameters: u_{fy} (yielding displacement), F_{fy} (yield strength), and b_f (strain-hardening ratio). The strain-hardening ratio, b_f, is the proportion of post-yield stiffness ($k_{f2}=b_f k_{f1}$) to the initial elastic stiffness ($k_{f1}=F_{fy}/u_{fy}$) with $F_{fy}=\mu_f N_f$. For this research, assumptions include u_{fy}=0.01 mm and b_f=10e-6, aiming to accurately replicate the rectangular hysteresis loop's characteristics regarding friction force at each cell versus displacement.

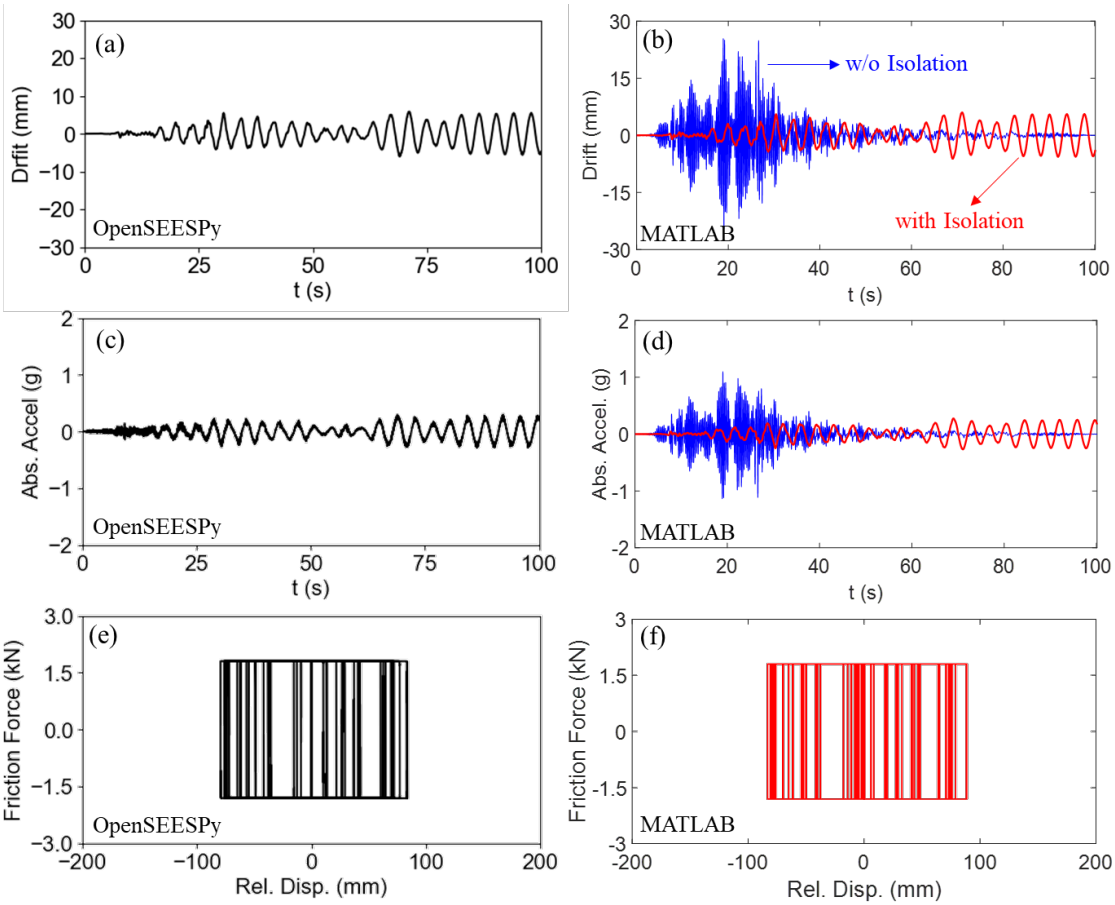

Figure 10. Comparison between the FE model and the numerical model of the proposed MI (N=4) created in MATLAB: (a,b) drift, (c,d) absolute acceleration of the primary mass, and (d,f) hysteresis loop of the friction force in cell 1.

A time history analysis is conducted to assess the performance of the MI when subjected to the ground motion record listed in Table 2. The following parameters are assumed for the MI: N=4, μ_c=0.5, μ_1=1.0, f_1=0.5, f_2=0.5, which corresponds to an optimized case described by Figures 5, 6, and 7. To evaluate the accuracy of the FE model, the results of this analysis are compared with those obtained from the numerical model presented in Section 4. Figure 10(a) depicts the time history of the base floor's drift as obtained from the FE model. Figure 10(a) is compared with Figure 10(b), which illustrates the time history of the same response, but as obtained from the numerical model, both with and without the MI for comparison. The results in both cases closely match, indicating the accuracy of the FE model developed using OpenSEESPy. Figures 10(c-d) and 10(e-f) compare the absolute acceleration of the primary mass and the force-displacement curve of the friction force in cell 1 (connected to the primary mass), respectively. In both cases, the FE model's results align very well with those from the numerical model, further validating the accuracy of the FE model.

5. CONCLUSIONS

This paper introduces a novel metamaterial isolator, named the Met-Isolator (MI), designed for the vibration isolation of civil structures. A solid friction is leveraged to augment its energy dissipation capacity. The proposed MI consists of multiple interconnected cells connected in series through a network of springs and dampers, where each cell includes a lumped mass, spring, damper, and sliding surface. A dynamic model is formulated to characterize the dynamic behavior of the proposed MI and optimize its vibration isolation and energy dissipation capabilities by minimizing the drift and absolute acceleration response of a single-story building. The key parameters involved include the mass and frequency ratios, the magnitude of the normal force acting on the sliding surface within each cell, and the number of cells. Furthermore, the accuracy of the proposed dynamic model is validated using a finite element model developed in OpenSEESPy. The numerical results indicate that the optimal performance achieved for lightweight MIs which happens when the cell frequency ratio approaches a value close to 0.5. In addition, the performance of lightweight MIs improves with an increase in the number of cells, whereas for heavier MIs, performance notably diminishes.

REFERENCES

[1] Al Rifaie, M., Abdulhadi, H. and Mian, A., "Advances in mechanical metamaterials for vibration isolation: A review," Advances in Mechanical Engineering **14**(3), 16878132221082872 (2022).

[2] Dalela, S., Balaji, P. S. and Jena, D. P., "A review on application of mechanical metamaterials for vibration control," Mechanics of Advanced Materials and Structures **29**(22), 3237–3262 (2022).

[3] Agrawal, A. K. and Amjadian, M., "Seismic component devices," [Innovative Bridge Design Handbook], Butterworth-Heinemann, 531–553 (2016).

[4] Vo, N. H., Pham, T. M., Hao, H., Bi, K. and Chen, W., "A reinvestigation of the spring-mass model for metamaterial bandgap prediction," International Journal of Mechanical Sciences **221**, 107219 (2022).

[5] Reynolds, M. and Daley, S., "An active viscoelastic metamaterial for isolation applications," Smart Mater. Struct. **23**(4), 045030 (2014).

[6] Wang, K., Zhou, J., Xu, D. and Ouyang, H., "Lower band gaps of longitudinal wave in a one-dimensional periodic rod by exploiting geometrical nonlinearity," Mechanical Systems and Signal Processing **124**, 664–678 (2019).

[7] Gao, F., Wu, Z., Li, F. and Zhang, C., "Numerical and experimental analysis of the vibration and band-gap properties of elastic beams with periodically variable cross sections," Waves in Random and Complex Media **29**(2), 299–316 (2019).

[8] Nauman Masoom, M., Ul Ain Karim, Q., Badar, I., Khushnood, R. A., Ahmed Najam, F. and Naseer, A., "Development of a new base isolation system using the concept of metamaterials," Engineering Structures **286**, 116151 (2023).

[9] Chondrogiannis, K. A., Dertimanis, V., Masri, S. and Chatzi, E., "Vibration absorption performance of metamaterial lattices consisting of impact dampers," 11 p. (2020).

[10] Lv, W., Yu, P. and Li, D., "An energy dissipation metamaterial based on Coulomb friction and vibration," International Journal of Mechanical Sciences **263**, 108764 (2024).

[11] Banerjee, A., Sethi, M. and Manna, B., "Vibration transmission through the frictional mass-in-mass metamaterial: An analytical investigation," International Journal of Non-Linear Mechanics **144**, 104035 (2022).

[12] Olsson, H., Åström, K. J., Canudas De Wit, C., Gäfvert, M. and Lischinsky, P., "Friction Models and Friction Compensation," European Journal of Control **4**(3), 176–195 (1998).

[13] Amjadian, M., "Vibration Control using Frictional Tuned Mass Dampers with Stick-Slip Motion," presented at IMAC-XLI - Society for Experimental Mechanics, 2023, Austin, TX.

[14] "MATLAB.", The MathWorks Inc. (2022).

[15] Ramallo, J. C., Johnson, E. A. and Spencer, B. F., "'Smart' Base Isolation Systems," Journal of Engineering Mechanics **128**(10), 1088–1099 (2002).

[16] Amjadian, M. and Haider, S. M. B., "Vibration control of a two-story base-isolated building using a new tuned mass multi-sliding friction damper," Active and Passive Smart Structures and Integrated Systems XVII, S. Tol, M. A. Nouh, S. Shahab, J. Yang, and G. Huang, Eds., 69, SPIE, Long Beach, United States (2023).

[17] PEER., "PEER Ground Motion Database," Shallow Crustal Earthquakes in Active Tectonic Regimes, NGA-West2 (2013).

[18] Hancock, J., Watson-Lamprey, J., Abrahamson, N. A., Bommer, J. J., Markatis, A., McCoy, E. M. M. A. and Mendis, R., "An improved method of matching response spectra of recorded earthquake ground motion using wavelets," Journal of Earthquake Engineering **10**(sup001), 67–89 (2006).
[19] ASCE., "Minimum design loads for buildings and other structures, ASCE 7-10" (2010).
[20] Zhu, M., McKenna, F. and Scott, M. H., "OpenSeesPy: Python library for the OpenSees finite element framework," SoftwareX **7**, 6–11 (2018).